

Vivid Structural Color Macropatterns Created by Flexible Nanopainting of Ultrafast Lasers

Yuhang Li, Xingyun Zhang, Tingting Zou,* Quanguan Mu, and Jianjun Yang*

Cite This: *ACS Appl. Mater. Interfaces* 2022, 14, 21758–21767

Read Online

ACCESS |



Metrics & More



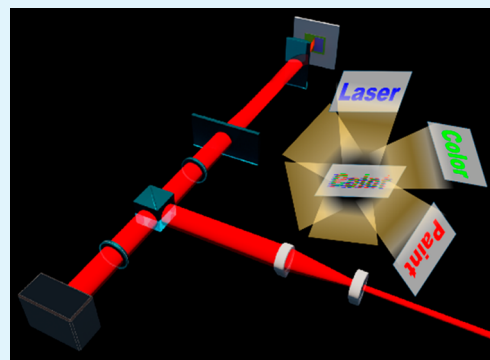
Article Recommendations



Supporting Information

ABSTRACT: Structural colors based on the macro- or nanostructure formation are ubiquitous in nature, having great prospects in many fields as a result of their environmentally friendly and long-term stable characteristics compared to pigments or dyes. However, the current fabrication techniques still face challenges for the generation of high-quality structural color patterns, especially at the macroscale, in an efficient way. Here, we demonstrate a method that exploits a flexible scanning process of generating macropatterns to convert the contour profiles into well-defined sub-micrometer grating structures with unprecedented vivid structural colors, at high speed and low cost on the graphene oxide film. The nature of dynamic beam shaping of the laser line spot allows us to flexibly construct the complex patterns at high speed, in sharp contrast to the traditional point-by-point laser processing. Moreover, the multicolor display of the patterns can be carried out by simply modulating the laser polarization to change the orientation of the sub-micrometer structures, and this nanopainting strategy is further explored to flexibly design the composite image for potential anti-counterfeiting applications.

KEYWORDS: structural color, laser-induced period surface structure, nanopainting, ultrafast laser, graphene oxide



INTRODUCTION

Color plays an important role in our daily life and work, and it can be mainly sourced to chemical (pigments and dyes) or physical (micro- and nanostructures and multilayer films) origins. The chemical pigments and dyes enrich the colors in the world ever since the first finding of the commercial synthetic dye in 1856.^{1,2} However, the low durability, pollution, and process complexity issues have brought challenges to their utilization. The physical-based structural colors have arisen from the light interaction with the spatially ordered sub-micrometer structures, which widely exist in natural biological systems.^{3–5} Since the electron microscope was introduced into biology in the 1940s,⁶ the artificial structural colors began to be investigated by researchers. The generation strategies of artificial structural colors, such as multilayer films, photonic crystals, metasurfaces, and diffraction gratings, have been widely studied over the past few decades,^{7–13} which demonstrate the structural color exhibiting unique properties of high brightness, fadeless appearance, eco-friendly management, and spectral tunability. It greatly enriches its utilization in both industry and research fields. Nowadays, structural colors have become a prominent choice in wide applications, such as visual aesthetic display, anti-counterfeiting, and multiplexed optical storage.^{10,12,14–17}

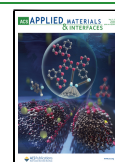
It has been proven that structural colors can be implemented by numerous high-precision fabrication techniques, including self-assembling, nanoimprinting, and lithography. The bottom-

up self-assembling is a cost-effective approach for the scalable production of structural colors. However, this method can only be arranged regularly along the substrate surface, which is a challenge for the arbitrary design and composite patterns.^{11,18} Nanoimprinting is also a mass-productive and high-resolution method, but it is difficult to become a general method as a result of the limitation of imprinting on flexible materials, such as polymers. Otherwise, it is susceptible to be damaged during the transfer process.^{13,19,20} Although focused electron or ion beam lithography enables the preparation of complex, high-precision structures, the fabrication is often confined within a very small scale as a result of the limitations of complicated procedures and high cost, leading to the structural color observation usually with the help of a microscope.^{15,21} In contrast to the aforementioned situations, the recent years of ultrafast laser manufacturing development strongly demonstrates its unique advantages in the structural color fabrication, showing a flexible, one-step, and contactless procedure and remarkably suitability for a wide scope of materials.^{12,22–28} The direct laser writing process is a prominent fabrication method,

Received: March 13, 2022

Accepted: April 21, 2022

Published: May 2, 2022



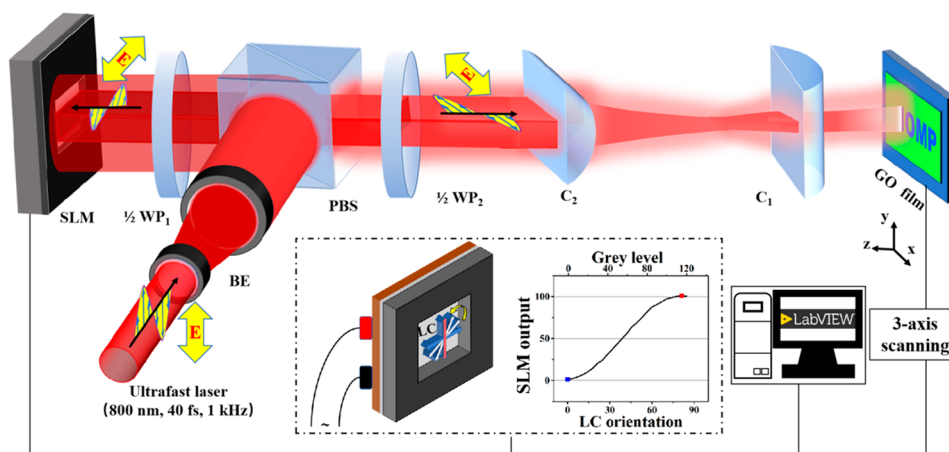


Figure 1. Configuration design for our presented FPS strategy. Here, E represents the linear polarization of the ultrafast laser beam, and BE represents a beam expander to enlarge the laser spot for adequately covering the facet of a SLM. The spatial intensity distribution of the laser beam is modulated by changing the liquid crystal (LC) orientations relative to the directions of the laser polarization. PBS stands for a polarized beam splitter, and $1/2\text{ WP}_1$ is a half waveplate for altering the laser polarization to guarantee the beam propagation through the PBS toward the focusing element. $1/2\text{ WP}_2$ is another half waveplate, which is used for rotating the direction of the laser polarization on the sample surface. C_1 and C_2 represent the cylindrical lenses. A homemade computer program is established to connect the three-axis scanning platform and the SLM operation.

producing nanostructures that are often featured with high resolution,^{17,29–31} and suitable for integration applications, such as optical storage. However, although a tight focus of the laser beam can act as a “pensile” to have a micro- or nanoscale fabrication in a mask-free and flexible way, the point-by-point processing still makes it confined, especially in work efficiency.^{32,33} The spatial light modulator (SLM) has been used by many research groups for ultrafast laser manufacturing with more efficiency.^{34,35} However, during such SLM-assisted laser processing, a tight focus of the laser beam spot was often demonstrated, which still limits its capability for further improvements.

On the other hand, the advanced development of laser-induced periodic surface structuring (LIPSS) would like to show great advantages in the efficient production of structural colors,^{23,26,36} because a group of periodic sub-micrometer-scale structure arrays rather than a single ablation pit or line can be miraculously created within the whole laser spot area, even without the restricted tight focusing conditions. Especially, through using a cylindrical lens for the line-shaped beam focusing, such a kind of laser fabrication can be equivalently considered as a “brush” to greatly improve the processing efficiency,^{27,37–39} which shows great potential for creating a large area of structural color at a high speed. Despite this, a cautiously optimistic outlook still remains, because its fabrication of the particular patterns often requires the assistance of hard masks, which consequently introduces some problems, such as the inconvenience of the mask changing, the color blurring on pattern edges, etc.^{24,38} Therefore, how to explore a high-speed flexible nanofabrication technique without hard masks is very much required for the high-quality structural color patterning.

We propose here a novel strategy to flexibly construct macropatterns with vivid structural colors at a high speed, by exploiting a computerized flexible nanopainting of structural colors (the so-called FPS) by ultrafast lasers on the graphene oxide (GO) film. The reason why we choose the GO material is due to its excellent physical and chemical properties in an air environment,^{40,41} so that a long-term durability of the structural color on the FPS pattern can be sustained. On the

other hand, the natural thin layer of GO material has excellent properties for transferring onto different substrates, such as rigid SiO_2 or soft polydimethylsiloxane (PDMS).^{42,43} This will help on the integration with other materials to promote its application in flexible display devices. The main principle of our solution relies on dividing the macropattern information into multiple slices for ultrafast laser-induced periodic sub-micrometer structures within a large line-shaped focal spot, assisted by a SLM to real-time change the beam intensity distribution. The laser irradiation process without additional hard masks can flexibly transfer the pattern designs on the sample surface by high-fidelity imprinting the periodic nanostructure arrays rather than a single ablation line appearance, via a combined cylindrical lens focusing system to eliminate the imaging problems of the sliced information. The spatial resolution of the laser nanopainted patterns can reach as high as 250 dpi. The observation of vivid structural colors with high brightness indicates the generation of unprecedentedly uniform nanostructures. The working efficiency of this method is about 2 min of time consumption for nanopainting of $1 \times 1\text{ cm}^2$ area. With consideration of the effectiveness of patterning and the resolution capability of human eyes, this work is well-suited to the application of a color display. More interestingly, such a technology can also be clearly identified for anti-counterfeiting and trademark printings, only through the flexible nanopainting of different patterns in the same macroscale area with the varying direction of the ultrafast laser polarizations.

RESULTS

Configuration and Design for FPS. Figure 1 demonstrates a schematic configuration of the FPS applied for the GO films. First, a commercial chirped pulse amplification femtosecond laser system (800 nm, 40 fs, and 1 kHz) is used as a light source, and its output laser beam is expanded via a pair of convex and concave lenses for providing a large spot with the less radical change of the intensity. Then, the laser with vertical linear polarization is reflected by the polarized beam splitter (PBS) onto a SLM, which can conveniently modify the intensity distribution of the laser to obtain a rapid maskless

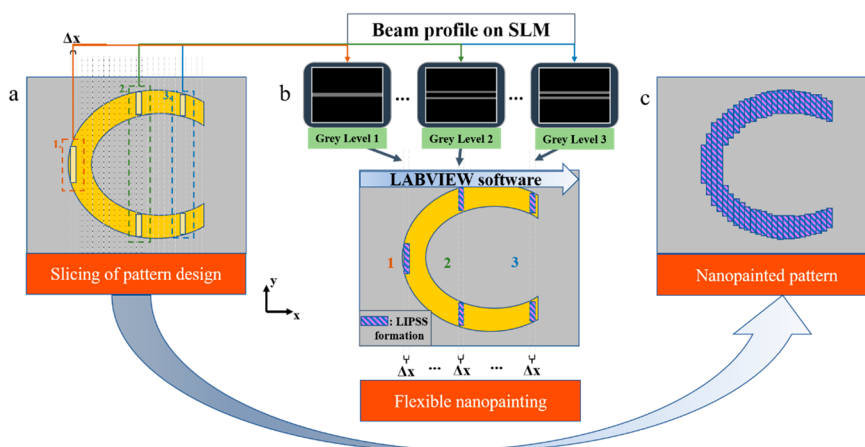


Figure 2. Principle of FPS by ultrafast laser irradiation. (a) Data slicing of a pattern “C”, where Δx is an interval width of each slice representing the spatial resolution in the x direction. (b) Dynamic beam shaping by the SLM for three different slices and their corresponding flexible nanopainting procedures. (c) FPS pattern of “C” is obtained by the line-by-line laser processing.

patterning on the sample surface. To make the modulated laser out of the SLM passes through the PBS, a half waveplate ($1/2 \text{ WP}_1$) is placed between the two items to transfer the laser polarization into a horizontal surface. After that, another half waveplate ($1/2 \text{ WP}_2$) is placed behind the PBS to adjust the laser polarization on the sample surface. For the purpose of achieving high-speed and large area nanofabrication, a cylindrical lens C_1 (with a focal length of $f_1 = 50 \text{ mm}$) is adopted for laser focusing, whose focal plane is located at the sample surface to obtain a line-shaped beam spot in the y direction, resulting in a large length-to-width ratio ($10 \text{ mm}/2.5 \mu\text{m} = 4000$). Under such circumstances, the spatial energy distribution of the linear focal spot is easily disturbed by the evident diffraction effect of the SLM facet, especially when the limited numbers of the pixels are selected for the dynamic modulation of the beam intensity.⁴⁴ In other words, the focal spot on the sample surface is not the conjugate imaging of the pattern on the SLM. To eliminate this problem, we insert another cylindrical lens C_2 (with a focal length of $f_2 = 150 \text{ mm}$) before C_1 to allow the sample surface to be located at the distance of $2f_2$, which consequently results in a conjugate plane of the SLM spatially overlapping with the focal plane of the femtosecond laser. Noticeably, within such a combined laser focusing system, the axial meridians of the two cylindrical lenses should be arranged perpendicular to each other, so that the diffraction of the focal spot energy along the y direction can be effectively avoided. The three-axis scanning platform is employed for the sample movement, which is connected to the SLM by LabVIEW software.

To demonstrate the principle of our femtosecond laser fabrication for the FPS, we select here the letter “C” to be an example, as shown in Figure 2. At first, the pattern design of “C” is disintegrated into data by many slices in the computer program (Figure 2a), because our laser processing is based on the irradiation of a line-shaped focal spot. This consequently leads to a so-called line-by-line processing instead of the traditional point-by-point processing. In fact, each divided slice of the pattern is ready to present a particular geometric profile, and its realization in the laser processing of course requires a corresponding intensity distribution of the focal spot, which is eventually achieved by the dynamic beam shaping on the SLM. Figure 2b shows the selection results of three slices in the pattern “C”, which are respectively located at the beginning,

middle, and end, to explain the conversion from the geometric profiles into the beam intensity modulations by the SLM. As a result, different variations of the gray levels are obtained in the y direction of the SLM facet for the three corresponding slices. Subsequently, the laser fabrication of each slice is carried out by the controllable movement of the sample surface, during which the LIPSSs are formed within the laser irradiation areas. Noticeably, the laser fabrication of different slices requires a fast switching of the SLM information and its accordance with the sample movement. In the experiment, this kind of synchronization between the sample position and the slice information is successfully performed by a homemade graphic user interface program. With the help of this real-time controlled computer program, the FPS of pattern “C” can be swiftly well-accomplished (Figure 2c). Through the line-by-line laser processing, we can achieve patterns even consisting of complex profiles within a large area of the surface. In other words, this configuration allows for flexible and rapid production of the arbitrary complex patterns by the sample scanning in one specific direction, in sharp contrast to the traditional meandering linewise scanning in the galvanometer scanner.

On the basis of the laser configuration and the synchronization program, we carried out the experiment of FPS. At first, the relations between the pixels of SLM and the fabrication width in the y direction on the sample surface should be identified (as shown in Figure S1 of the Supporting Information), which are critical to the parameter settings for a desirable ablation length. Clearly, the pixels generated by the SLM show excellent linearity in the y direction with the patterns produced on the GO surface, and the required minimum number of the pixels on the SLM is found as $N = 8$ for a pattern formation. This provides a fundamental assurance for the subsequent patterning with high accuracy control. Panels a and b of Figure 3 show the optical images of the typically nanopainted results, where both patterns are processed with the laser power of $P = 235 \text{ mW}$ after the SLM reflection and a scanning speed of $v = 0.25 \text{ mm s}^{-1}$, from which the accumulative pulses can be calculated by $N_{\text{eff}} = (D \times f) / v = 10$.⁴⁵ As a result, it is clear that the “CIOMP” and “UCAS” patterns tend to display different bright monochromatic colors (green and blue, respectively) when they are viewed from distinct angles. Especially, their pure colors

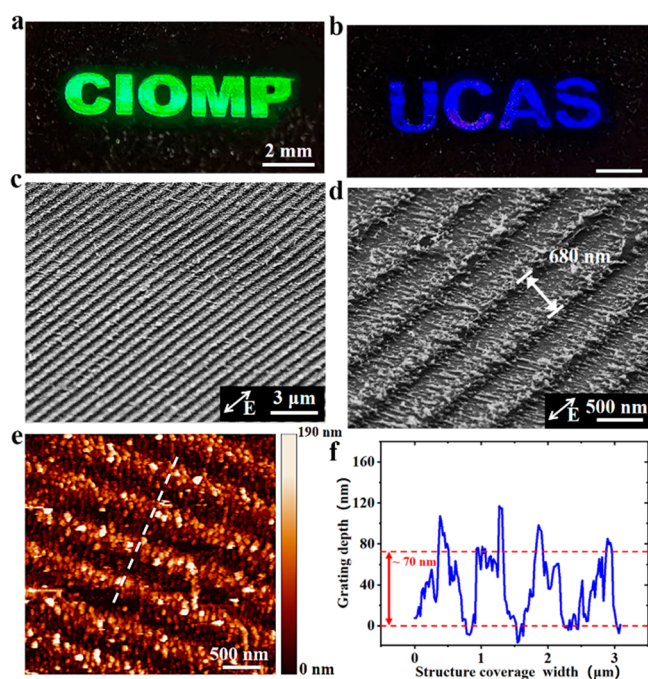


Figure 3. Typical results for the simple FPS patterns. (a and b) Observation of structural colors for the nanopainted patterns of “CIOMP” and “UCAS” on the GO films. (c and d) SEM image shows that the grating orientation is parallel to the polarization of the laser, and its period is ~ 680 nm. (e and f) AFM analysis shows that the depth of the grating structure is ~ 70 nm.

display in somewhat degree indicates the uniform formation of these macropatterns. The fabrication procedure is presented in [Movie S1](#) of the Supporting Information, which shows a one-step maskless laser processing in a rapid way. Including the operation time of the LabVIEW program, the total time consumption for the fabrication of the colorful “CIOMP” and “UCAS” patterns approximates only 40 s. Panels c and d of [Figure 3](#) illustrate the measured high-resolution images of the patterns with scanning electron microscopy (SEM), in which the highly regular distribution of the grating structures (or LIPSSs) is generated with the spatial period of about $\Lambda = 680$ nm. Moreover, we also find that the periodic grating structures are oriented parallel to the direction of the laser polarization. According to our previous studies, the formation mechanism of such regular LIPSSs is attributed to the TE-mode surface wave excitation under ultrafast laser irradiation.^{38,39} The fast Fourier transform (FFT) results in [Figure S2](#) of the Supporting Information provide the confirmation of our sub-micrometer grating structures with the improved distribution uniformity in comparison to the previous report.⁴⁶ Afterward, the surface morphology of the patterns is characterized via atomic force microscopy (AFM) (panels e and f of [Figure 3](#)), and it is seen that the average fluctuation depth of the grating structures approximates $h = 70$ nm. Conclusively, the line scanning of the ultrafast laser on the sample surface is not only to generate the contour profiles of the macroscale pictures but also to produce the highly uniform distribution of the LIPSSs inside. It is the optical response of the latter that makes the whole pattern display vivid colors.

Angle-Dependent Color Display of the FPS. In fact, the optical response of the periodic sub-micrometer grating structures can be quantitatively evaluated by a diffraction equation²²

$$d(\sin(i) + \sin(\theta)) = m\lambda \quad (1)$$

where d represents the grating period, i and θ are the incident and diffraction angles, and m is the diffraction order, respectively. When a white light illuminates on the patterned sample surface, different wavelengths included will be spatially separated through the optical diffraction in variable directions. Therefore, we can observe the distinct colors on the pattern at different viewing angles of θ .

For a given incident light within a wavelength range of $\lambda = 300$ – 800 nm and FPS patterns consisting of the periodic sub-micrometer grating structures, we calculate the diffraction wavelengths at different orders, as shown in [Figure 4b](#). The 0 order stands for the light reflection including the full wavelengths. The diffraction wavelengths at the first order range from $\lambda = 300$ to 680 nm, while the diffraction at the second order has a maximum wavelength at about $\lambda = 340$ nm. Considering the visibility of the structure colors, we choose the first-order diffraction lights for the color display investigation.

Here, the laser-induced pattern of “CIOMP” (in [Figure 3b](#)) is selected for the practical implementation of the angle-dependent structural color display. The experimental configuration is made up of a colorized charge-coupled device (CCD) camera, a light-emitting diode (LED) light source, and a sample holder ([Figure 4a](#)). The well-collimated white light illuminates the sample surface along the normal direction, i.e., $i = 0^\circ$. The colorized CCD camera is placed in the y - z plane allowing for the maximum brightness of the structural colors. As shown in [Figure 4c](#), when the CCD camera changes its viewing angles from $\theta = 40^\circ$ to 80° , the “CIOMP” pattern can present abundant structural colors varying among blue, green, yellow, and red. The dependence of the available structural colors upon the viewing angle of θ is marked in CIE 1931, as shown in [Figure 4d](#). Clearly, the contour line of our obtained structural colors substantially covers the commercial imaging standard, or the structural colors displayed by the pattern become more enriched. Furthermore, the comparison of the measurements to the calculation results for the angle-dependent structural color is also shown in [Figure 4e](#), where the consistent tendency indicates the homogeneous distribution of the sub-micrometer grating structures contained in the FPS patterns. It also exhibits enriched colors at different diffraction angles.

FPS for the Macroscale Complex Designs. In addition to the simple English letters, we further exploit this configuration for some macroscale patterns, including complex information, during which the direction of the laser polarization (or the spatial orientation of the induced sub-micrometer grating structures) is maintained identical at all places. For example, [Figure 5a](#) shows the reflected image of a FPS logo for the Changchun Institute of Optics, Fine Mechanics and Physics (CIOMP) of the Chinese Academy of Sciences, where both the complicated geometry and Chinese characters are involved. The production of this logo with an area of 9×9 mm² spends a total time of about 110 s. The other two pictures correspond to the observations at two viewing angles of $\theta = 55^\circ$ and 60° , respectively, which accordingly display different structural colors.

More interestingly, another FPS pattern for a quick response (QR) code is also successfully implemented, as shown in [Figure 5b](#). During this laser fabrication, the QR code, downloaded from the internet, is then transformed into a soft mask via the LabVIEW program to modulate the intensity

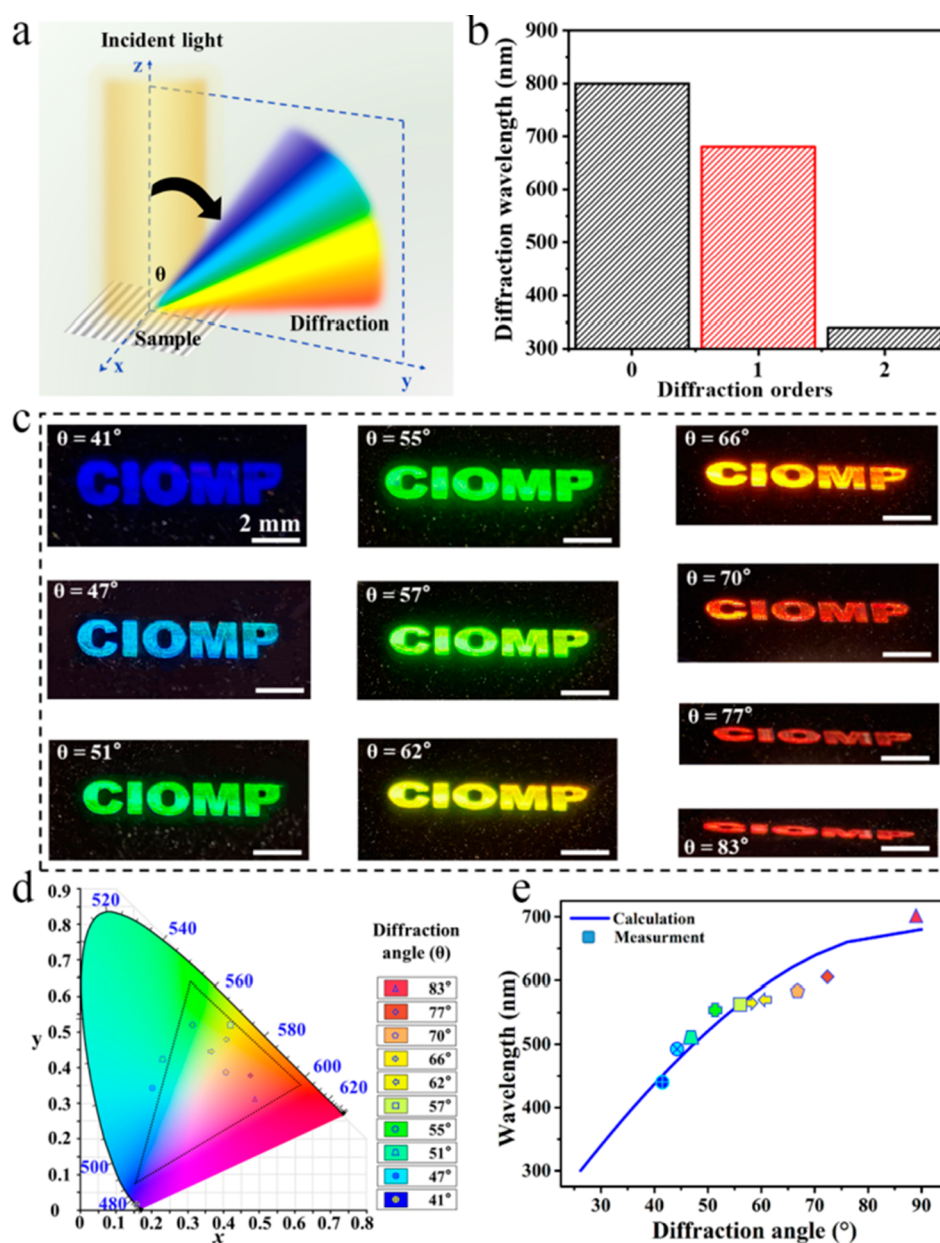


Figure 4. Angle-dependent characterization of the color display effect for the FPS patterns. (a) Schematic diagram of the experimental setup for the angle-dependent observation of the structural colors. The illumination light is placed above the sample to provide an incident angle of $i = 0^\circ$, and the diffraction lights at different angles of θ within the y - z plane that are perpendicular to the grating orientation can be monitored by a CCD camera. (b) Calculated wavelengths observed at different diffraction orders for the incident light within a wavelength range of $\lambda = 300$ – 800 nm. (c) Observation of the angle-dependent structural colors for the FPS pattern of “CIOMP”. (d) Our obtained colorization is marked in the CIE 1931. The triangle with a black dotted line is the commercial imaging standard. (e) Observed wavelengths (only for the first-order diffraction) as a function of the diffraction angle for the incident lights ranging from $\lambda = 300$ to 680 nm.

distribution of the laser beam spot. During the sample scanning process, the sub-micrometer grating structures are generated on the laser irradiation area of the sample surface. The total time consumption for the fabrication area of 6.5×6.5 mm² reaches approximately 50 s. In this laser-fabricated QR code, the minimum interval between the two adjacent structured regions is about 4 pixels, corresponding to a minimum length of 50 μ m for the area without the laser irradiation, while the minimum length of the structured region is about 8 pixels, thus leading to a high image resolution of 250+ dpi, which represents a prominent quality in the paper-printing or color-spraying situations. Of course, such a high-

quality FPS code can display intriguing structural colors when they are viewed from different angles. Remarkably, the prepared FPS QR code can be easily read by a commercial smartphone to acquire the corresponding information.

FPS Composites for the Multicolor Display. As a matter of fact, through altering the direction of the laser polarization during the sample scanning process, we can also make the laser-induced sub-micrometer grating structures within different parts of the composite present distinguishable orientations, so that they can display different structural colors, even at the same viewing angle. As shown in Figure 6a, during our design, a butterfly pattern is separated into three parts (I, II, and III)

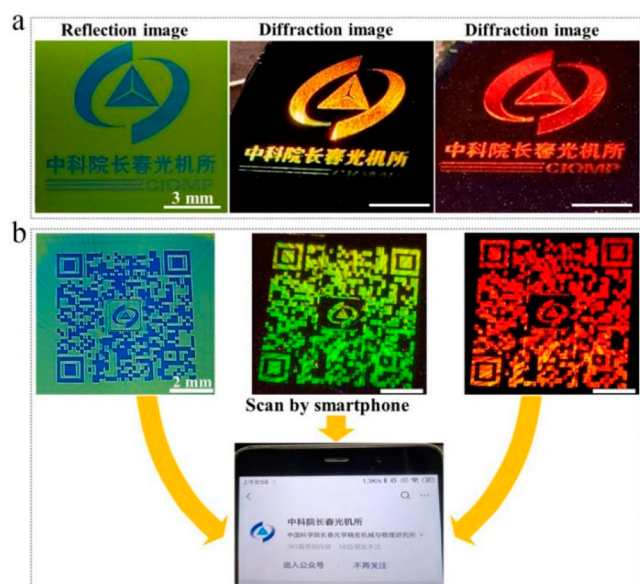


Figure 5. Achieved macroscale FPS with complex designs. (a) Reflection and diffraction images for a FPS logo of CIOMP, Chinese Academy of Sciences. (b) Reflection and diffraction images for a FPS QR code and its scanning usability.

by considering their different gray values, and each part is scanned by the ultrafast laser irradiation with variable laser polarizations, thus leading to different spatial orientations for the correspondingly induced periodic sub-micrometer grating structures. The specific processing scheme for each step and the processing results are shown in Figure S3 of the Supporting Information. Subsequently, the colorized display of the butterfly pattern is characterized by two observation schemes with different illumination options, where an azimuth angle of the sample position, φ , is defined as zero when the grating orientation within part I is arranged parallel to the x axis, and its value increases with rotating the sample platform counter-clockwise. For the illumination with the collimated light, when the diffraction viewing angle is given by $\theta = 50^\circ$, we can visualize three parts of the butterfly composite to respectively show the green colors at different azimuth angles of $\varphi = 0^\circ$, 20° , and 40° , as shown in Figure 6b. In this case, they are seen in a separate way, owing to the different designs in the sub-micrometer grating orientations. On the other hand, according to eq 1, when the light illumination is replaced by two light sources from different directions, the observation at the certain diffraction angle is deemed to have two different wavelengths because of variable incident angles for two light sources, leading to the vivid surface coloring of the micropattern with LIPSSs. Of course, the appearance of the structural colors seems to be varied with changing the incident angles of the light illumination, as shown in Figure 6c. Thus, it is fascinating to find that the whole butterfly pattern can be visualized with multiple colors, even at the same viewing angle.

Composited FPS for Image Hiding. Inspired by the aforementioned multicolor display with variable orientations of the periodic grating structures, we further explore its potential in the information hiding via fabricating different patterns in the same macroscale surface area. As shown in Figure 7a, a composited FPS is designed for image hiding, where the words “Laser”, “Paint”, and “Color” present three images, and each of them is fabricated with different orientations (0° , 40° , and 80°)

of the LIPSSs. In other words, the details of each image are transformed onto the GO film with the particularly oriented sub-micrometer grating structures. These images are separated in the micro-level but totally overlapped in the same macroscale surface. As a result, the achieved FPS of the emblem is shown in Figure 7a (in the lower right corner), where three images are unable to obtain direct identification because of their spatial locking with each other in the same macro-area.

The decoding of these three images with the corresponding structural colors requires the display configuration in Figure 6a. When the FPS of the emblem is illuminated by the LED light source at normal incidence, the three images become spatially unlocked with varying both θ and φ angles, as shown in Figure 7b. For example, when the azimuth angle is fixed as $\varphi = 0^\circ$, we can only see the pattern of “Laser” nanopainted on the GO film, which displays the blue, green, and red colors at the viewing angles of $\theta = 45^\circ$, 50° , and 60° , respectively. Similarly, both the “Paint” and “Color” patterns can be seen separately at the sample azimuth angles of $\varphi = 40^\circ$ and 80° , respectively, whose structural colors are correspondingly varied with different θ values. Movie S2 of the Supporting Information shows the excellent image hiding effects of such a FPS composite at the viewing angle of $\theta = 50^\circ$ when the azimuth angle of φ continuously changes by rotating the sample platform. We only demonstrate here nine decoding modes based on a variety of colors and patterns. As a matter of fact, this kind of method can be feasible for the design of more patterns in the composited FPS pattern.

DISCUSSION

The flexible nanopainting strategy provides a capability for the rapid maskless fabrication of the complex patterns in a macroscale range, and the obtained FPS patterns can display the vivid single and multiple structural colors through the optical diffraction of the sub-micrometer grating structures involved. In particular, because of the highly uniform formation of the periodic gratings, the corresponding structural color display becomes purified and substantially covers the commercial imaging standard. More interestingly, through the active manipulation of the induced grating orientation for different parts of the pattern, the composited FPS can be clearly shown for both the full-color display and image hiding, which have great potential in anti-counterfeiting applications.

In general, such an ultrafast laser nanopainting technology is not just limited to GO films. It can also be applied to other materials, such as metals and semiconductors. As shown in Figure S4 of the Supporting Information, FPSs are well-generated on both tungsten (W) and silicon (Si) surfaces, indicating the extendable capability of our proposed technology in practice. Additionally, three characteristic parameters of the LIPSS, including the depth, the period, and the distribution regularity, can all affect the quality of surface colorizing. In practice, however, the variation of the LIPSS depth is often only in a range of a few tens of nanometers; thus, its influence on the color brightness can be neglected. Because the structure arrangement regularity affects the saturation of the brightness, the irregular formation of LIPSS will lead to the disordered surface colorizing in the brightness change. The LIPSS period is definitely an essential factor to influence the chromaticity of surface colorizing, which can be modulated using different incident laser wavelengths.⁴⁷ This means that the observation of more rich and

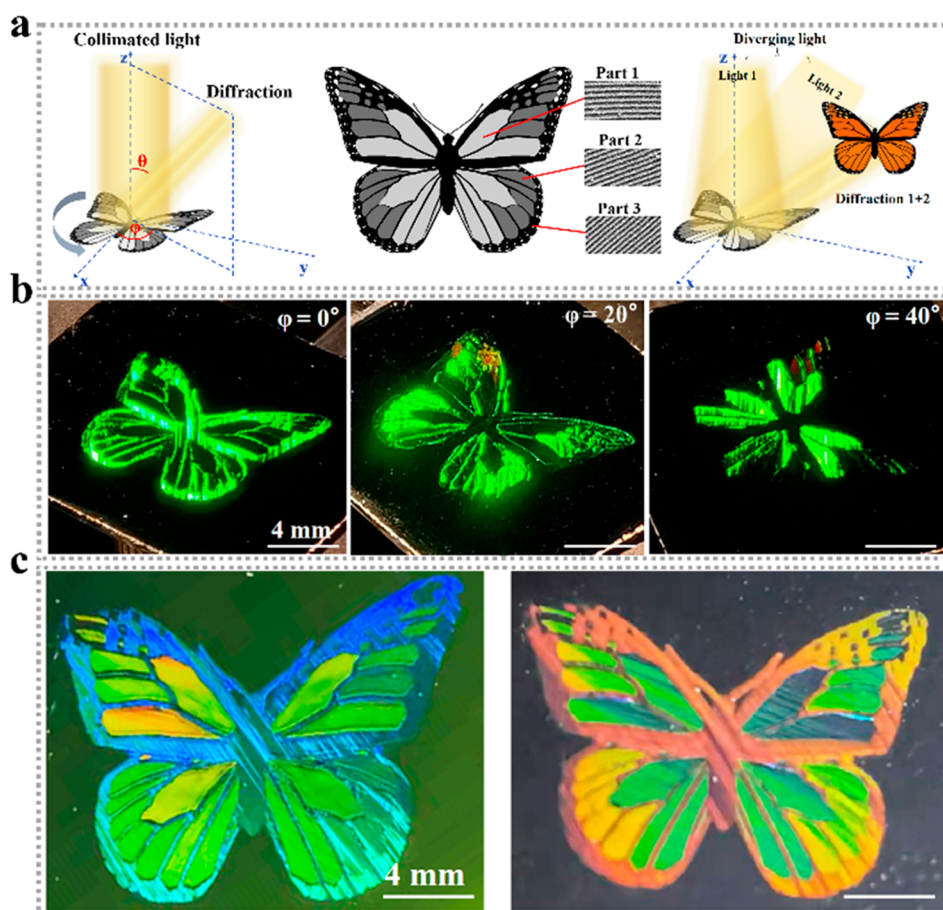


Figure 6. Characterization of a FPS butterfly composite. (a) Three parts of the laser fabrication design for multiple structural colors and two types of observation schemes for the FPS composite. Grayscales for different parts (I, II, and III) of the butterfly are represented by the LIPSS with variable orientations. φ is defined as an angle between the grating orientation of part I and the x direction. (b) Viewing results of the FPS butterfly composite at $\varphi = 0^\circ$, 20° , and 40° , respectively, when the diffraction angle is given by $\theta = 50^\circ$. (c) Combination of two light sources with different incident angles is used as a diverging light illumination above the sample surface. The FPS butterfly composite demonstrates the vivid multiple structural colors under the illumination of the divergent light source.

polychromatic colors at the same viewing angle can be further achieved through designing the LIPSS pattern with different periods. However, this technology is still facing a few challenges that need to be tackled. For example, for a composited FPS, the current spatial resolution for each image cannot reach the high values because of the pixel occupation for multiple patterns, which can be compensated by either the correction of higher order aberrations or reducing the sizes of the liquid crystal molecules. For the macroscale of the FPS, the fabrication size in the vertical direction is in fact limited by the length of the Gaussian laser beam spot line-focused by two cylindrical lenses. In future research, it is reasonable to increase the vertical size of FPS by the further expansion of the laser beam onto a larger facet SLM and using the beam-shaping technology to turn the Gaussian beam into a flat-top profile.

CONCLUSION

In summary, we have developed a novel flexible nanopainting strategy of an ultrafast laser for the efficient construction of macroscale patterns with vivid structural colors. By the real-time control of the SLM for the laser intensity shaping and the sample movement for the generation of the periodic sub-micrometer grating structures, the sliced pattern design can be

accordingly nanoimprinted on the GO film, thus leading to the optical diffraction for the structural color evidence. In comparison to the traditional point-by-point laser fabrication, our FPS fabrication has used a combination of two cylindrical lenses and a SLM modulation process to obtain a line-shaped focusing laser spot, which lays a foundation for the high-speed processing in the macroscales. This maskless nanopainting has been proven more flexible and efficient, even for complex patterns, and its work efficiency can be on the order of centimeters per minute. Moreover, our obtained structural colors seem to be more enriched and substantially cover the commercial imaging standard.

More importantly, through the flexible production of the sub-micrometer grating structures with variable orientations, different patterns can be identified to integrate together in either the macro- or microscale for the multicolor composite image or information hiding, respectively. In general, our method has proposed a new approach to achieve the color marking with the substantial improvement in both the fabrication efficiency and coloring quality, which provides prospects for the information steganography and anti-counterfeiting solution.

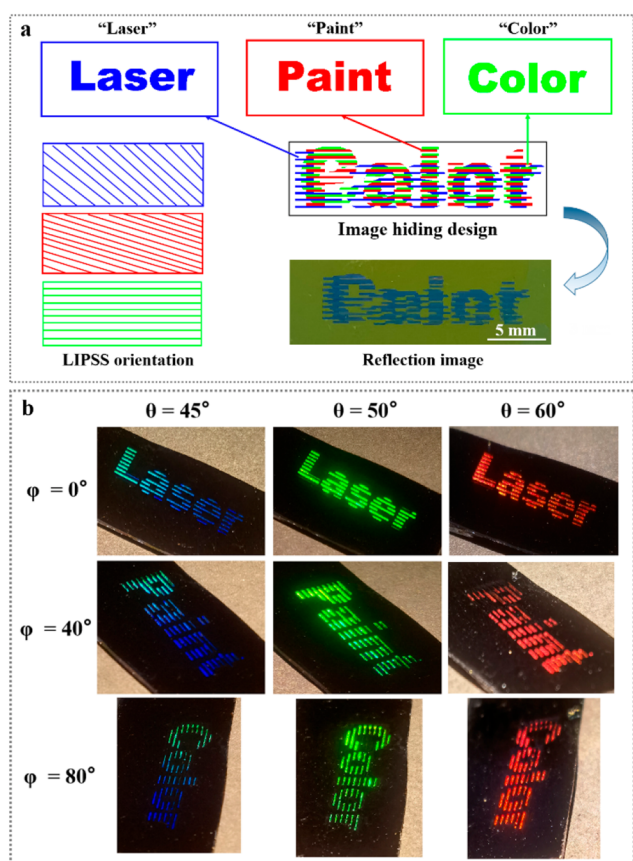


Figure 7. Potential application of the composited FPS in anti-counterfeiting of the image. (a) Design and fabrication of the hiding FPS images “Laser”, “Paint”, and “Color” within the same macroscale area. (b) Photographs of the FPS emblem from different viewing angles of θ and ϕ , showing three decoding images.

EXPERIMENTAL SECTION

Materials. Hummer-method-modified GO is introduced into the experiment. GO is dispersed and dissolved in deionized water to prepare a uniform GO dispersion (1.5 mg mL^{-1}). The surface of the Si (300 nm SiO_2) substrate is transferred into hydrophilicity under the oxygen plasma treatment. The GO dispersion is rotated onto the Si/SiO₂ substrate through a spin-coating approach (2400 r for 25 s) to obtain a thin GO film. The film depth is controlled by accumulating the dips of GO dispersion on the substrate. The thickness of the GO film is about 80 nm after spin coating about 30 times (Figure S5 of the Supporting Information).

Femtosecond Laser Fabrication. The FPS patterns can be swiftly processed using a commercial chirped pulse amplification femtosecond laser system (Spitfire Ace, Spectra Physics), which delivers the laser pulses with the central wavelength of 800 nm and the pulse width of 40 fs at the repetition rate of 1 kHz. The employed laser power for the formation of FPS is $P = 235 \text{ mW}$, which is measured after the laser beam reflection from the SLM facet without the modification of the laser beam. A cylindrical optical lens is applied to generate a line-shaped focal spot on the sample surface. The energy of laser pulses is adjusted by a combination of the Glan–Tylor prism and the half-wave plate. The maximum scanning speed is $v = 0.25 \text{ mm s}^{-1}$, and the compressed width of the focal line on the scanning direction D is $2.5 \text{ }\mu\text{m}$, leading to the pulse numbers of $N_{\text{eff}} = 10$ overlapped within the laser spot area. The modification of the laser intensity is carried out through a spatial light modulator (Hamamatsu LCoS-SLM X13138). The controlling and synchronizing systems are implemented via a homemade LabVIEW program.

Characterization. The optical images are captured by a confocal microscope (Keyence VK-X1000). The detailed surface morphologies are characterized by SEM (Phenom, Eindhoven, Netherlands) and AFM (Bruker, Billerica, MA, U.S.A.). The structural colors of the laser nanopainted sample are taken by a commercial scientific CCD camera (Thorcam 4070C) accompanied by a C-mount lens (DH-MH2520M).

ASSOCIATED CONTENT

Supporting Information

The Supporting Information is available free of charge at <https://pubs.acs.org/doi/10.1021/acsami.2c04542>.

Relationship between the used pixels displayed on the SLM screen and the corresponding fabrication length (Figure S1), FFT analysis of the sub-micrometer grating structures (Figure S2), constituents of the orientation-based butterfly FPS according to the grayscale and its fabrication process (Figure S3), generation of FPS on different materials for (a–d) W and (e–h) Si surfaces (Figure S4), and thickness of the GO film on the SiO₂/Si substrate (Figure S5) (PDF)

FPS fabrication process with 8 times acceleration (MP4) Image hiding effect on the FPS with different structure directions under the same observation condition (MP4)

AUTHOR INFORMATION

Corresponding Authors

Tingting Zou – GPL Photonics Laboratory, Changchun Institute of Optics, Fine Mechanics and Physics (CIOMP), Chinese Academy of Sciences (CAS), Changchun, Jilin 130033, People’s Republic of China; Email: zoutingting@ciomp.ac.cn

Jianjun Yang – GPL Photonics Laboratory, Changchun Institute of Optics, Fine Mechanics and Physics (CIOMP), Chinese Academy of Sciences (CAS), Changchun, Jilin 130033, People’s Republic of China; orcid.org/0000-0002-6703-4403; Email: jjyang@ciomp.ac.cn

Authors

Yuhang Li – GPL Photonics Laboratory, Changchun Institute of Optics, Fine Mechanics and Physics (CIOMP), Chinese Academy of Sciences (CAS), Changchun, Jilin 130033, People’s Republic of China; Center of Materials Science and Optoelectronics Engineering, University of Chinese Academy of Sciences, Beijing 100049, People’s Republic of China

Xingyun Zhang – State Key Laboratory of Applied Optics, Changchun Institute of Optics, Fine Mechanics and Physics (CIOMP), Chinese Academy of Sciences (CAS), Changchun, Jilin 130033, People’s Republic of China

Quanquan Mu – State Key Laboratory of Applied Optics, Changchun Institute of Optics, Fine Mechanics and Physics (CIOMP), Chinese Academy of Sciences (CAS), Changchun, Jilin 130033, People’s Republic of China

Complete contact information is available at: <https://pubs.acs.org/10.1021/acsami.2c04542>

Notes

The authors declare no competing financial interest.

ACKNOWLEDGMENTS

This research was financially supported by the K. C. Wong Education Foundation (GJTD-2018-08) and the National Natural Science Foundation of China (Grant 91750205).

■ ABBREVIATIONS USED

FPS, flexible nanopainting of structural colors; SLM, spatial light modulator; LC, liquid crystal; PBS, polarized beam splitter; 1/2 WP₁, half waveplate 1; 1/2 WP₂, half waveplate 2; GO, graphene oxide; BE, beam expander; LIPSS, laser-induced periodic surface structure

■ REFERENCES

- (1) Clarke, E.; Anliker, R. *Anthropogenic Compounds*; Springer: Berlin, Germany, 2013; Vol. 3, pp 181.
- (2) Gonzaga, L. A.; Santana, V. T.; Bernardi, M. I. B.; Hruby, J.; Neugebauer, P.; Mesquita, A. CeO(2) and CeO₂:Pr Nanocrystalline Powders Prepared by The Polymeric Precursor Method: Yellow and Red Pigments with Tunable Color. *J. Am. Ceram. Soc.* **2020**, *103* (11), 6280–6288.
- (3) Vukusic, P.; Sambles, J. R. Photonic Structures in Biology. *Nature* **2003**, *424* (6950), 852–5.
- (4) Teyssier, J.; Saenko, S. V.; van der Marel, D.; Milinkovitch, M. C. Photonic Crystals cause Active Colour Change in Chameleons. *Nat. Commun.* **2015**, *6* (1), 6368.
- (5) McCoy, D. E.; Feo, T.; Harvey, T. A.; Prum, R. O. Structural Absorption by Barbule Microstructures of Super Black Bird of Paradise Feathers. *Nat. Commun.* **2018**, *9* (1), 1.
- (6) Anderson, T. F.; Richards, A. G. An Electron Microscope Study of Some Structural Colors of Insects. *J. Appl. Phys.* **1942**, *13* (12), 748–758.
- (7) Wood, B.; Pendry, J. B.; Tsai, D. P. Directed Subwavelength Imaging Using a Layered Metal-dielectric System. *Phys. Rev. B* **2006**, *74* (11), 115116.
- (8) Kristensen, A.; Yang, J. K. W.; Bozhevolnyi, S. I.; Link, S.; Nordlander, P.; Halas, N. J.; Mortensen, N. A. Plasmonic Colour Generation. *Nat. Rev. Mater.* **2017**, *2* (1), 16088.
- (9) Li, Y. C.; Fan, Q. S.; Wang, X. H.; Liu, G. J.; Chai, L. Q.; Zhou, L.; Shao, J. Z.; Yin, Y. D. Shear-Induced Assembly of Liquid Colloidal Crystals for Large-Scale Structural Coloration of Textiles. *Adv. Funct. Mater.* **2021**, *31* (19), 2010746.
- (10) Deng, J.; Deng, L.; Guan, Z.; Tao, J.; Li, G.; Li, Z.; Li, Z.; Yu, S.; Zheng, G. Multiplexed Anticounterfeiting Meta-image Displays with Single-Sized Nanostructures. *Nano Lett.* **2020**, *20* (3), 1830–1838.
- (11) Liu, X. J.; Wang, J. J.; Tang, L. H.; Xie, L. J.; Ying, Y. B. Flexible Plasmonic Metasurfaces with User-Designed Patterns for Molecular Sensing and Cryptography. *Adv. Funct. Mater.* **2016**, *26* (30), 5515–5523.
- (12) Sharma, N.; Vangheluwe, M.; Vocanson, F.; Cazier, A.; Bugnet, M.; Reynaud, S.; Vermeulin, A.; Destouches, N. Laser-driven Plasmonic Gratings for Hiding Multiple Images. *Mater. Horiz.* **2019**, *6* (5), 978–983.
- (13) Zheng, J.; Ye, Z. C.; Wang, C. L.; Fu, Y. F.; Huang, X. R.; Sheng, Z. M. Highly Tunable Polarized Chromatic Plasmonic Films Based on Subwavelength Grating Templates. *Adv. Mater. Technol.* **2019**, *4* (5), 1800661.
- (14) Li, K. X.; Li, T. Y.; Zhang, T. L.; Li, H. Z.; Li, A.; Li, Z.; Lai, X. T.; Hou, X. Y.; Wang, Y.; Shi, L.; Li, M. Z.; Song, Y. L. Facile Full-color Printing with a Single Transparent Ink. *Sci. Adv.* **2021**, *7* (39), No. eabh1992.
- (15) Huo, P.; Song, M.; Zhu, W.; Zhang, C.; Chen, L.; Lezec, H. J.; Lu, Y.; Agrawal, A.; Xu, T. Photorealistic Full-color Nanopainting Enabled by Low-loss Metasurface. *Optica* **2020**, *7* (9), 1171–1172.
- (16) Zijlstra, P.; Chon, J. W.; Gu, M. Five-dimensional Optical Recording Mediated by Surface Plasmons in Gold Nanorods. *Nature* **2009**, *459* (7245), 410–3.
- (17) Qiao, M.; Yan, J. F.; Jiang, L. Direction Controllable Nano-Patterning of Titanium by Ultrafast Laser for Surface Coloring and Optical Encryption. *Adv. Opt. Mater.* **2022**, *10*, 2101673.
- (18) Liu, P. M.; Bai, L.; Yang, J. J.; Gu, H. C.; Zhong, Q. F.; Xie, Z. Y.; Gu, Z. Z. Self-assembled Colloidal Arrays for Structural Color. *Nanoscale Adv.* **2019**, *1* (5), 1672–1685.
- (19) Kikuchi, T.; Nishinaga, O.; Natsui, S.; Suzuki, R. O. Polymer Nanoimprinting using an Anodized Aluminum Mold for Structural Coloration. *Appl. Surf. Sci.* **2015**, *341*, 19–27.
- (20) Kumar, K.; Duan, H.; Hegde, R. S.; Koh, S. C. W.; Wei, J. N.; Yang, J. K. W. Printing Colour at the Optical Diffraction Limit. *Nat. Nanotechnol.* **2012**, *7* (9), 557–561.
- (21) Li, Z. L.; Chen, C.; Guan, Z. Q.; Tao, J.; Chang, S.; Dai, Q.; Xiao, Y.; Cui, Y.; Wang, Y. Q.; Yu, S. H.; Zheng, G. X.; Zhang, S. Three-Channel Metasurfaces for Simultaneous Meta-Holography and Meta-Nanoimprinting: A Single-Cell Design Approach. *Laser Photonics Rev.* **2020**, *14* (6), 2000032.
- (22) Dusser, B.; Sagan, Z.; Soder, H.; Faure, N.; Colombier, J. P.; Jourlin, M.; Audouard, E. Controlled Nanostructures Formation by Ultra Fast Laser Pulses for Color Marking. *Opt. Express* **2010**, *18* (3), 2913–24.
- (23) Reinhardt, H.; Kim, H. C.; Pietzonka, C.; Kruempelmann, J.; Harbrecht, B.; Roling, B.; Hampp, N. Self-organization of Multifunctional Surfaces-the Fingerprints of Light on a Complex System. *Adv. Mater.* **2013**, *25* (24), 3313–8.
- (24) Wu, H.; Jiao, Y.; Zhang, C.; Chen, C.; Yang, L.; Li, J.; Ni, J.; Zhang, Y.; Li, C.; Zhang, Y.; Jiang, S.; Zhu, S.; Hu, Y.; Wu, D.; Chu, J. Large Area Metal Micro-/Nano-groove Arrays with Both Structural Color and Anisotropic Wetting Fabricated by One-step Focused Laser Interference Lithography. *Nanoscale* **2019**, *11* (11), 4803–4810.
- (25) Huang, J.; Jiang, L.; Li, X. W.; Wang, A. D.; Wang, Z.; Wang, Q. S.; Hu, J.; Qu, L. T.; Cui, T. H.; Lu, Y. F. Fabrication of Highly Homogeneous and Controllable Nanogratings on Silicon via Chemical Etching-assisted Femtosecond Laser Modification. *Nanophotonics* **2019**, *8* (5), 869–878.
- (26) Soldera, M.; Fortuna, F.; Teutoburg-Weiss, S.; Milles, S.; Taretto, K.; Lasagni, A. F. Comparison of Structural Colors Achieved by Laser-Induced Periodic Surface Structures and Direct Laser Interference Patterning. *J. Laser Micro/Nanoeng.* **2020**, *15* (2), 97–103.
- (27) Cao, K.; Chen, L.; Cheng, K.; Sun, Z.; Jia, T. Regular Uniform Large-area Subwavelength Nanogratings Fabricated by the Interference of Two Femtosecond Laser Beams via Cylindrical Lens. *Chin. Opt. Lett.* **2020**, *18* (9), 093201.
- (28) Chowdhury, S. N.; Nyga, P.; Kudyshev, Z. A.; Garcia Bravo, E.; Lagutchev, A. S.; Kildishev, A. V.; Shalae, V. M.; Boltasseva, A. Lithography-free Plasmonic Color Printing with Femtosecond Laser on Semicontinuous Silver Films. *ACS Photonics* **2021**, *8* (2), 521–530.
- (29) Roberts, A. S.; Novikov, S. M.; Yang, Y.; Chen, Y.; Boroviks, S.; Beermann, J.; Mortensen, N. A.; Bozhevolnyi, S. I. Laser Writing of Bright Colors on Near-percolation Plasmonic Reflector Arrays. *ACS Nano* **2019**, *13* (1), 71–77.
- (30) Wang, X.; Kuchmizhak, A.; Storozhenko, D.; Makarov, S.; Juodkakis, S. Single-step Laser Plasmonic Coloration of Metal Films. *ACS Appl. Mater. Interfaces* **2018**, *10* (1), 1422–1427.
- (31) Wu, P.; Cao, X.; Zhao, L.; Chen, Z.; Zhang, M.; Juodkakis, S.; Zhang, W. Dynamic Structural Color Display Based on Femtosecond Laser Variable Polarization Processing. *Adv. Mater. Interfaces* **2021**, *8* (16), 2100460.
- (32) Mizeikis, V.; Purlys, V.; Buividas, R.; Juodkakis, S. Realization of Structural Color by Direct Laser Write Technique in Photoresist. *J. Laser Micro/Nanoeng.* **2014**, *9* (1), 42.
- (33) Jiang, S.; Hu, Y.; Wu, H.; Zhang, Y.; Zhang, Y.; Wang, Y.; Zhang, Y.; Zhu, W.; Li, J.; Wu, D.; Chu, J. Multifunctional Janus Microplates Arrays Actuated by Magnetic Fields for Water/Light Switches and Bio-Inspired Assimilatory Coloration. *Adv. Mater.* **2019**, *31* (15), No. 1807507.
- (34) Xu, Z.; Jiang, L.; Li, X.; Wang, A.; Li, B.; Huang, L.; Lin, Z.; Huang, J.; Lu, Y. Flash Ablation of Tunable and Deep-Subwavelength Nanogap by Using a Spatially Modulated Femtosecond Laser Pulse for Plasmonic Application. *ACS Appl. Nano Mater.* **2019**, *2* (8), 4933–4941.
- (35) Kontenis, G.; Gailevičius, D.; Jonušauskas, L.; Purlys, V. Dynamic Aberration Correction via Spatial Light Modulator (SLM)

for Femtosecond Direct Laser Writing: Towards Spherical Voxels. *Opt. Express* **2020**, *28* (19), 27850–27864.

(36) Livakas, N.; Skoulas, E.; Stratakis, E. Omnidirectional Iridescence Via Cylindrically-polarized Femtosecond Laser Processing. *Opto-Electron. Adv.* **2020**, *3* (5), 190035.

(37) Wang, L.; Chen, Q. D.; Cao, X. W.; Buividas, R.; Wang, X.; Juodkazis, S.; Sun, H. B. Plasmonic Nano-printing: Large-area Nanoscale Energy Deposition for Efficient Surface Texturing. *Light: Sci. Appl.* **2017**, *6* (12), No. e17112.

(38) Zou, T.; Zhao, B.; Xin, W.; Wang, Y.; Wang, B.; Zheng, X.; Xie, H.; Zhang, Z.; Yang, J.; Guo, C. L. High-speed Femtosecond Laser Plasmonic Lithography and Reduction of Graphene Oxide for Anisotropic Photoresponse. *Light: Sci. Appl.* **2020**, *9* (1), 69.

(39) Zou, T. T.; Zhao, B.; Xin, W.; Wang, F. Y.; Xie, H. B.; Li, Y. H.; Shan, Y. W.; Li, K.; Sun, Y. B.; Yang, J. J. Birefringent Response of Graphene Oxide Film Structurized via Femtosecond Laser. *Nano Res.* **2021**, 1–10.

(40) Wang, Y.; Li, S. S.; Yang, H. Y.; Luo, J. Progress in the Functional Modification of Graphene/Graphene Oxide: A Review. *RSC Adv.* **2020**, *10* (26), 15328–15345.

(41) Wu, J.; Jia, L.; Zhang, Y.; Qu, Y.; Jia, B.; Moss, D. J. Graphene Oxide for Integrated Photonics and Flat Optics. *Adv. Mater.* **2021**, *33* (3), No. 2006415.

(42) Zheng, X.; Jia, B.; Lin, H.; Qiu, L.; Li, D.; Gu, M. Highly Efficient and Ultra-broadband Graphene Oxide Ultrathin Lenses with Three-dimensional Subwavelength Focusing. *Nat. Commun.* **2015**, *6* (1), 8433.

(43) Jiang, H. B.; Liu, Y. Q.; Zhang, Y. L.; Liu, Y.; Fu, X. Y.; Han, D. D.; Song, Y. Y.; Ren, L.; Sun, H. B. Reed Leaf-Inspired Graphene Films with Anisotropic Superhydrophobicity. *ACS Appl. Mater. Interfaces* **2018**, *10* (21), 18416–18425.

(44) Senior, T. B. A. Half Plane Edge Diffraction. *Radio Sci.* **1975**, *10* (6), 645–650.

(45) Bonse, J.; Mann, G.; Krüger, J.; Marcinkowski, M.; Eberstein, M. Femtosecond Laser-induced Removal of Silicon Nitride Layers from Doped and Textured Silicon Wafers used in Photovoltaics. *Thin Solid Films* **2013**, *542*, 420–425.

(46) Gnilitzky, I.; Derrien, T. J.-Y.; Levy, Y.; Bulgakova, N. M.; Mocek, T.; Orazi, L. High-speed Manufacturing of Highly Regular Femtosecond Laser-induced Periodic Surface Structures: Physical Origin of Regularity. *Sci. Rep.* **2017**, *7* (1), 8485.

(47) Puerto, D.; Garcia-Lechuga, M.; Hernandez-Rueda, J.; Garcia-Leis, A.; Sanchez-Cortes, S.; Solis, J.; Siegel, J. Femtosecond Laser-controlled Self-assembly of Amorphous-crystalline Nanogratings in Silicon. *Nanotechnology* **2016**, *27* (26), 265602.

Recommended by ACS

Assembly of Nanometer-Sized Hollow Sphere Colloidal Crystals for Applications as Tunable Photonic Materials

Chia-Hua Hsieh, Hongta Yang, *et al.*

OCTOBER 07, 2022
ACS APPLIED NANO MATERIALS

READ 

Predicting Laser-Induced Colors of Random Plasmonic Metasurfaces and Optimizing Image Multiplexing Using Deep Learning

Hongfeng Ma, Nathalie Destouches, *et al.*

JUNE 03, 2022
ACS NANO

READ 

3D Optical Heterostructure Patterning by Spatially Allocating Nanoblocks on a Printed Matrix

Kaixuan Li, Yanlin Song, *et al.*

SEPTEMBER 12, 2022
ACS NANO

READ 

All-Optical Tunability of Metalenses Permeated with Liquid Crystals

Giovanna Palermo, Giuseppe Strangi, *et al.*

OCTOBER 10, 2022
ACS NANO

READ 

Get More Suggestions >